Letters

An Underwater Simultaneous Wireless Power and Analog–Digital Hybrid Signal Transfer System

Bo Luo, Mengyao Wang, Jie Tang, Tiantian Wang, Longlei Bai, and Jiang You

***Abstract*—An underwater simultaneous wireless power and analog–digital hybrid signal transfer system is proposed in this letter to meet the needs of analog and digital signal transmission in underwater sensor networks in seawater. The system transmits two digital signals and one analog signal through the same coil, meeting the practical needs of multiple signal transmissions, improving the communication rate, and retaining the precision and continuity of analog signals as well as the accuracy of digital signals. The system uses a coaxial coil coupling structure, with the outer ring for power transmission and the inner ring for signal transmission, featuring a simple and compact design. The experimental platform achieved a 400 W output power, 1 Mbps bidirectional digital signal transmission, and 20 kHz unidirectional analog signal transmission in seawater, with a transmission efficiency of 90.8%, verifying the feasibility of the proposed theory.**

***Index Terms*—Analog–digital hybrid signal transmission, coaxial coils, simultaneous wireless power and data transfer (SWPDT), wireless power transfer.**

I. Introduction

WIRELESS power transfer has been increasingly adopted in underwater power supply applications, such as unmanned underwater vehicles and deep-sea sensors, owing to its flexibility, safety, and convenience [1], [2]. To enhance the system's efficiency and stability, power transmission should be integrated with information interaction, including control feedback signals and real-time monitoring data exchange.

Conventional electromagnetic communication methods (e.g., Wi-Fi, Zigbee, and Bluetooth) exhibit high latency and severe signal attenuation in underwater environments. To overcome these limitations, researchers have developed various simultaneous wireless power and data transfer (SWPDT) schemes, which can be classified into two strategies based on coil-sharing configurations. The first strategy utilizes all or part of the power channel's coupled coils for data transmission. For example, Wu et al. [3] employed the entire power channel's coupled coils for communication, whereas Li et al. [4] injected a high-frequency data carrier into a subsection of the power coil using a tap method. While this approach improves system integration and flexibility, it introduces higher interference and operational complexity. The differences in carrier frequency and current magnitude between the power and communication channels lead to different requirements for the parameters of the Litz wire. The second strategy adopts separate coupled coils for power and data channels. Da et al. [5], for instance, implemented double-D-shaped (DD) coils for power transmission and Q coils for communication. This configuration reduces transmission difficulty and cross-channel interference but increases structural complexity. In addition, the square shape of the double-D quadrature (DDQ) coils leads to an uneven magnetic field distribution, which can cause energy losses.

Existing studies on SWPDT focus exclusively on digital transmission, which is insufficient for control systems requiring real-time analog feedback. For example, underwater sensors can transmit continuous analog signals (e.g., temperature and pressure) [6] to the power supply device, while simultaneously exchanging control data between the sensor and the power supply device. Digital-only solutions impose strict analog-to-digital converter (ADC) tradeoffs: high sampling rates waste bandwidth, while low rates lead to signal distortion. Higher ADC resolution improves accuracy but increases power consumption. This approach not only degrades analog signal fidelity but also raises system complexity and bandwidth demands.

Considering the above challenges, this letter proposes an underwater simultaneous wireless power and analog–digital hybrid signal transmission system with the following three key contributions. 1) A novel analog–digital mixed-signal SWPDT system is proposed, which allows digital signals and analog signals to be independently transmitted after digital modulation and analog modulation, respectively. It reduces the additional ADC module, occupies a small bandwidth, and maintains the accuracy and continuity of the signal. 2) A planar coaxial coupled coil design with separate power/ communication coils, offering easy fabrication, reduced crosstalk, and improved stability. 3) Experimental validation showing 400 W power transfer, 1 Mbps bidirectional digital communication, and 20 kHz analog transmission.

II. System Overview

Fig. 1 shows the schematic diagram of the proposed underwater simultaneous wireless power and analog–digital hybrid

Received 22 April 2025; revised 14 May 2025, 6 June 2025, and 3 July 2025; accepted 17 July 2025. Date of publication 22 July 2025; date of current version 8 September 2025. This work was supported in part by the National Natural Science Foundation of China under Grant 52307006 and in part by the Yantai Science and Technology Innovation Development Plan under Grant 2024JCYJ084. *(Corresponding author: Longlei Bai.)*

The authors are with Yantai Research Institute, Harbin Engineering University, Yantai 264000, China (e-mail: longlei0107@hrbeu.edu.cn).

Color versions of one or more figures in this article are available at https://doi.org/10.1109/TPEL.2025.3591528.

Digital Object Identifier 10.1109/TPEL.2025.3591528

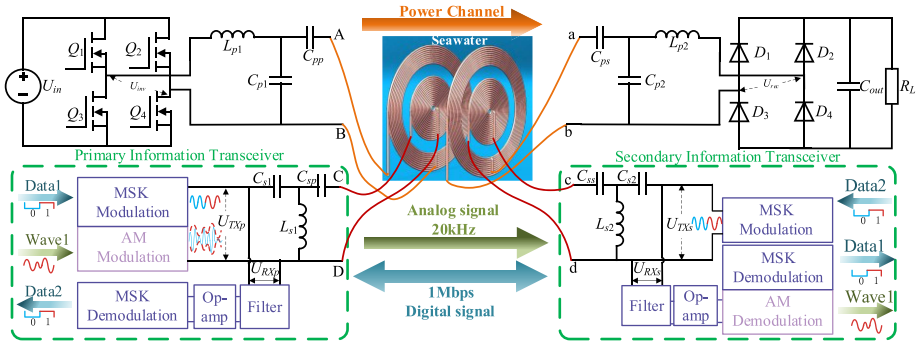

Fig. 1. Schematic diagrams of the proposed system.

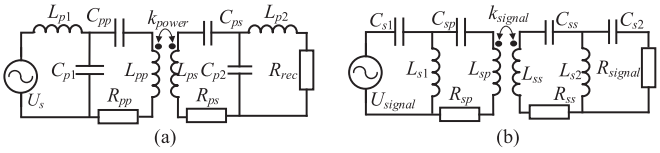

Fig. 2. Equivalent circuit. (a) Power channel. (b) Communication channel.

signal transmission system. The system consists of a power channel and a communication channel, where the inner and outer rings of the coaxial coil are employed for power and signal transmission, respectively. The power channel utilizes a double-sided LCC compensation network to achieve constant current output and block high-frequency communication signals [7]. The communication channel employs a dual-sided capacitor-inductor-capacitor network (*CLC*) compensation network to enhance communication carrier transmission and isolate power interference [8].

The resonant frequency of the power channel is much lower than the communication frequency, resulting in high impedance at communication frequencies. Compared with the current transmitted by the power channel, the current induced in the power coil by the communication channel is very small, and the impact of the communication carrier on power transmission is negligible. However, the power carrier induces a significant current in the communication coil, interfering with communication transmission. Therefore, it is necessary to reduce the crosstalk from the power channel to the communication channel.

A. Power Channel

This letter utilizes the superposition theorem for circuit analysis. When analyzing the power channel independently, the equivalent circuit is presented in Fig. 2(a). In this configuration, R_{pp} and R_{ps} denote the equivalent internal resistances of the power coils, encompassing both the ac internal resistances and the eddy current losses induced by the coils in seawater. The compensation topology satisfies the following conditions:

$$\begin{cases} \omega_{\mathrm{p}} L_{\mathrm{p1}} = 1/(\omega_{\mathrm{p}} C_{\mathrm{p1}}), \omega_{\mathrm{p}} L_{\mathrm{p2}} = 1/(\omega_{\mathrm{p}} C_{\mathrm{p2}}) \\ \omega_{\mathrm{p}} L_{\mathrm{pp}} = 1/(\omega_{\mathrm{p}} C_{\mathrm{p1}}) + 1/(\omega_{\mathrm{p}} C_{\mathrm{pp}}) \\ \omega_{\mathrm{p}} L_{\mathrm{ps}} = 1/(\omega_{\mathrm{p}} C_{\mathrm{p2}}) + 1/(\omega_{\mathrm{p}} C_{\mathrm{ps}}). \end{cases} \tag{1}$$

B. Communication Channel

For the isolated analysis of the communication channel, Fig. 2(b) depicts the equivalent circuit model of the signal transmission path. R_{sp} and R_{ss} denote the equivalent internal resistances of the communication coils, comprising both the ac internal resistances and the eddy current losses induced by the coils in seawater. To simplify analysis and design, the communication channel's circuit parameters are designed to be symmetrical. To ensure the stability and reliability of the communication system, the carrier frequency for forward digital signal transmission is used as the resonant frequency for circuit design. The carrier frequency for forward data transmission is selected as ω_{s}, and expressed as follows:

$$\begin{cases} \omega_{\mathrm{s}} L_{\mathrm{s1}} = 1/(\omega_{\mathrm{s}} C_{\mathrm{s1}}), \omega_{\mathrm{s}} L_{\mathrm{s2}} = 1/(\omega_{\mathrm{s}} C_{\mathrm{s2}}) \\ \omega_{\mathrm{s}} L_{\mathrm{s1}} + \omega_{\mathrm{s}} L_{\mathrm{sp}} = 1/(\omega_{\mathrm{s}} C_{\mathrm{sp}}) \\ \omega_{\mathrm{s}} L_{\mathrm{s2}} + \omega_{\mathrm{s}} L_{\mathrm{ss}} = 1/(\omega_{\mathrm{s}} C_{\mathrm{ss}}). \end{cases} \tag{2}$$

Fig. 3 shows the frequency response characteristics of the circuit gain G_{s} versus coil inductance L and operating frequency f. The results indicate that G_{s} exhibits a negative value at the power carrier frequency f_{p}, while demonstrating a positive value at the communication frequency f_{s}. Furthermore, G_{s} maintains high gain levels for frequencies above f_{s}. These characteristics verify that the dual-sided *CLC* compensation network effectively enhances data carrier transmission while suppressing power interference.

C. Digital–Analog Hybrid Signal Transmission System

The signal transmission scheme of the proposed system is shown in Fig. 4. The system utilizes minimum shift keying (MSK) modulation for digital signals and amplitude modulation (AM) for continuous monitoring signals, as illustrated in Fig. 5(a) and (b). The digital signals are modulated by the field-programmable gate array (FPGA), while the analog signals are processed by the signal generator. These modulated signals are then connected to C_{s1} and combined at the input of the communication *CLC* topology to form a composite signal source. Through careful selection of different carrier frequencies, the two signal types occupy separate frequency bands, enabling simultaneous transmission via frequency division multiplexing. At the receiver, the composite signals are separated in the

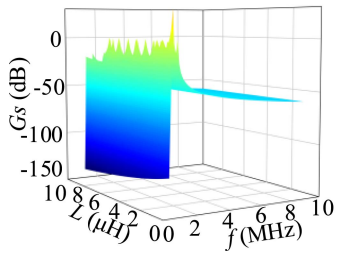

Fig. 3. Influence of parameters on G_s. ($R_{sp} = R_{ss} = 237\ \Omega$, $L_{sp} = 8.28\ \mu$H, $L_{ss} = 8.07\ \mu$H, and $R_{signal} = 20\ k\Omega$).

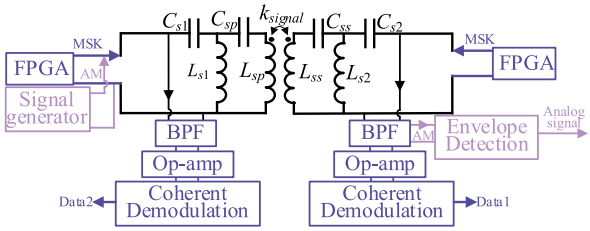

Fig. 4. Analog–digital signal hybrid transmission scheme.

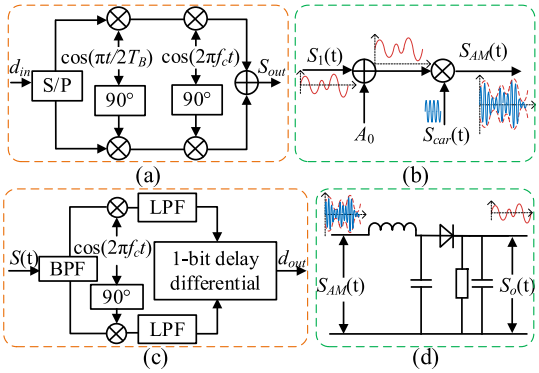

Fig. 5. Process of signal modulation and demodulation. (a) MSK modulation. (b) AM modulation. (c) MSK coherent demodulation. (d) AM envelope detection demodulation.

frequency domain, filtered to remove noise components, and demodulated through MSK and AM demodulation processes shown in Fig. 5(c) and (d), respectively. The bandwidth of the MSK modulated signal is $1.5\times R_b$. R_b is the symbol transmission rate. The bandwidth of the AM modulated signal is $2\times f_{max}$. f_{max} is the highest frequency of the analog signal.

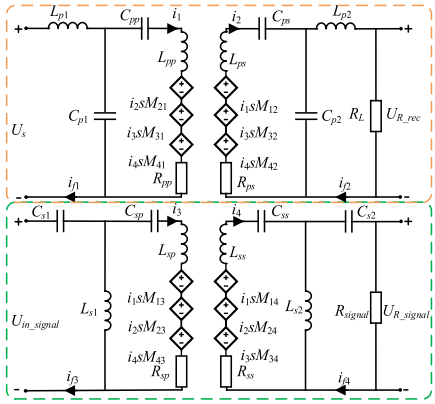

Fig. 6. Equivalent mathematical model of system.

D. Analysis of Power Interference on Communication

Fig. 6 reveals mutual interference phenomena between power and communication coils, as indicated by the mutual inductance parameters $M_{13}(M_{31})$, $M_{14}(M_{41})$, $M_{23}(M_{32})$, and $M_{24}(M_{42})$. The analysis primarily focuses on power channel-induced interference affecting the communication channel.

The voltage–current relationship can be derived as expressed in (3), where A denotes the coefficient matrix. The current vector I and voltage vector V are mathematically represented by (5) and (6), respectively

$$\mathbf{AI} = \mathbf{V} \tag{3}$$

Equation (4), shown at the bottom of this page.

$$\mathbf{I} = [i_2,\ i_3,\ i_4,\ i_{f1},\ i_{f2},\ i_{f3},\ i_{f4}]^{\mathbf{T}} \tag{5}$$

$$\mathbf{V} = [U_S,\ U_{\text{in\_signal}},\ 0,\ 0,\ 0,\ 0,\ 0,\ 0]^{\mathrm{T}}. \tag{6}$$

In which

$$\begin{cases} a = 1/sC_{pp} + sL_{pp} + R_{pp} + 1/sC_{p1} \\ b = 1/sC_{ps} + sL_{ps} + R_{ps} + 1/sC_{p2} \\ c = sL_{p2} + R_L + 1/sC_{p2} \\ d = 1/sC_{sp} + sL_{sp} + R_{sp} + sL_{s1} \\ e = 1/sC_{ss} + sL_{ss} + R_{ss} + sL_{s2} \\ f = 1/sC_{s2} + R_{signal} + sL_{s2}. \end{cases} \tag{7}$$

$$A = \begin{bmatrix} -1/sC_{p1} & 0 & 0 & 0 & sL_{p1} + 1/(sC_{p1}) & 0 & 0 & 0 \\ 0 & 0 & -sL_{s1} & 0 & 0 & 0 & sL_{s1} + 1/(sC_{s1}) & 0 \\ a & sM_{21} & sM_{31} & sM_{41} & -1/(sC_{p1}) & 0 & 0 & 0 \\ -sM_{12} & b & -sM_{32} & -sM_{42} & 0 & -1/(sC_{p2}) & 0 & 0 \\ 0 & -1/(sC_{p2}) & 0 & 0 & 0 & c & 0 & 0 \\ sM_{13} & sM_{23} & d & sM_{43} & 0 & 0 & -sL_{s1} & 0 \\ -sM_{14} & -sM_{24} & -sM_{34} & e & 0 & 0 & 0 & -sL_{s2} \\ 0 & 0 & 0 & -sL_{s2} & 0 & 0 & 0 & f \end{bmatrix}. \tag{4}$$

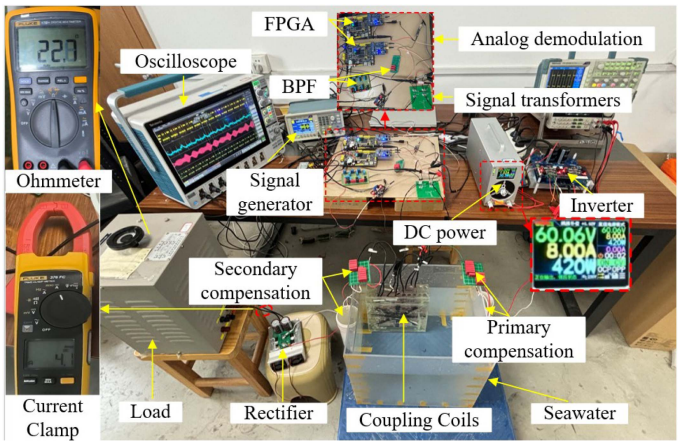

Fig. 7. Experimental platform.

To simplify the system design, the circuit parameters on both sides are designed to be symmetrical

$$\begin{cases} L_{\mathrm{pp}} = L_{\mathrm{ps}} = L_1, L_{\mathrm{sp}} = L_{\mathrm{ss}} = L_2 \\ L_{\mathrm{p1}} = L_{\mathrm{p2}} = L_3, L_{\mathrm{s1}} = L_{\mathrm{s2}} = L_4 \\ C_{\mathrm{p1}} = C_{\mathrm{p2}} = C_1, C_{\mathrm{pp}} = C_{\mathrm{ps}} = C_2 \\ C_{\mathrm{s1}} = C_{\mathrm{s2}} = C_3, C_{\mathrm{sp}} = C_{\mathrm{ss}} = C_4 \\ R_{\mathrm{pp}} = R_{\mathrm{ps}} = R_1, R_{\mathrm{sp}} = R_{\mathrm{ss}} = R_2. \end{cases} \tag{8}$$

Therefore, $a = b$ and $d = e$. Using Cramer's rule, the solution to the equation can be found. Let $s = j{\cdot}\omega_{\mathrm{p}}$, and from (3), the power-to-data interference coupling can be derived as follows:

$$\left|\frac{U_{\mathrm{R\_signal}}(j\omega_p)}{U_s(j\omega_p)}\right| = \frac{R_{\mathrm{signal}}}{|A|} {L_2}^2 {L_1}^2 (j\omega_p)^2 \frac{L_4 L_3}{\sqrt{L_1 L_2}} \cdot |B|$$

$$\approx k \cdot \left(1 + \frac{L_4}{L_2}\right) \sqrt{(R_L k_{12} k_{24})^2 + \left[k_{14}\left(\frac{R_1 R_L}{\omega_p L_1} + \frac{{L_3}^2 \omega_p}{\sqrt{L_1}}\right)\right]^2}. \tag{9}$$

Matrix B is represented as (10), shown at the bottom of this page. Among them, $k = \frac{s^2 R_{\mathrm{signal}} L_4}{|A_1| C_1 C_3}$ and $|A_1| = \frac{|A|}{L_1 \sqrt{L_1} L_2 \sqrt{L_2}}$.

To ensure communication gain G_{s} and power transmission efficiency, L_1– L_4, R_{L}, and R_1 remain constant, and k is a constant. From the simplified results, the main interference to the communication part comes from the direct effect k_{14}, and the indirect effect k_{12}, k_{24} from the power primary coil to the power secondary coil and then to the communication secondary coil. To improve power transmission efficiency, k_{12} should be increased.

TABLE I
PARAMETER VALUES FOR PROPOSED SYSTEM

Parameters	Values
L_{pp}, L_{ps}, L_{sp}, and L_{ss} (μH)	35.9, 36.1, 19.0, and 20.7
L_{p1}, L_{p2}, L_{s1}, and L_{s2} (μH)	20, 20, 1, and 1
M_{p} and M_{s} (μH)	16 and 10.11
C_{pp}, C_{ps}, C_{p1}, C_{p2}, C_{s1}, and C_{s2} (nF)	622, 622, 500, 500, 1.5, and 1.5
C_{sp} and C_{ss} (pF)	75 and 75
R_{pp}, R_{ps}, R_{sp}, R_{ss}, and R_{L} (Ω)	0.088, 0.107, 237, 237, and 22.7
f_{p}, f_{df}, f_{dr}, and f_{a}	50 kHz, 4 MHz, 9 MHz, and 17 MHz
U_{d}	60.06 V
Date rate (Forward/Backward)	1 Mbps, 1 Mbps
Analog signal frequency	20 kHz

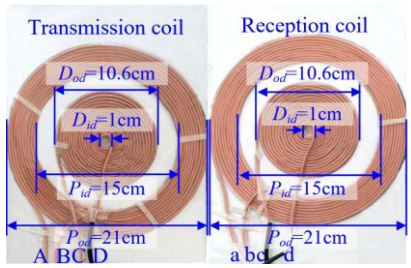

Fig. 8. Planar coaxial coils.

At the same time, to reduce the impact of power transmission on the communication channel, k_{24} and k_{14} can be decreased. By increasing the distance between the power and communication coils on the same plane, the coupling coefficients k_{24} and k_{14} are reduced.

III. EXPERIMENTAL RESULTS AND COMPARISON

A. Experimental Setup

To verify the feasibility of the proposed underwater SWPDT system, an experimental platform is established, as shown in Fig. 7. The experiment used simulated seawater with conductivity of 5.8 S/m, and the water temperature was maintained at around 25 °C. The experiment was conducted in an indoor water tank with dimensions of 40 cm × 30 cm × 40 cm, and the height of the simulated seawater was approximately 28 cm.

For the communication channel, ZYNQ-7000 FPGAs are used. The coil distance is 2 cm. The parameters of the power and communication channels are shown in Table I. Fig. 8 is the front view of the coaxial coil. Points A (a), B (b), C (c), and D (d) correspond to the nodes in Fig. 1. To reduce interference between

$$B = \begin{bmatrix} 0 & 1/(j\omega_{\mathrm{p}} \cdot C_3) + j\omega_{\mathrm{p}} \cdot L_4 & 0 & 0 & -(j\omega_{\mathrm{p}} \cdot L_4)/\sqrt{L_2} \\ (j\omega_{\mathrm{p}} \cdot L_3)/\sqrt{L_1} & 0 & -j\omega_{\mathrm{p}} \cdot k_{12} & R_1/L_1 & -j\omega_{\mathrm{p}} \cdot k_{23} \\ R_L & 0 & 0 & (j\omega_{\mathrm{p}} \cdot L_3)/\sqrt{L_1} & 0 \\ 0 & -(j\omega_{\mathrm{p}} \cdot L_4)/\sqrt{L_2} & j\omega_{\mathrm{p}} \cdot k_{13} & j\omega_{\mathrm{p}} \cdot k_{23} & 1/(j\omega_{\mathrm{p}} \cdot C_4 \cdot L_2) + j\omega_{\mathrm{p}} + R_2/L_2 + j\omega_{\mathrm{p}} \cdot (L_4/L_2) \\ 0 & 0 & -j\omega_{\mathrm{p}} \cdot k_{14} & -j\omega_{\mathrm{p}} \cdot k_{24} & -j\omega_{\mathrm{p}} \cdot k_{34} \end{bmatrix}. \tag{10}$$

TABLE II
COMPARISON WITH PREVIOUS WORK

Reference	[4]	[8]	[9]	[10]	[11]	Proposed
P_{out}	1 kW	23.1 W	1 kW	40 W	220 W	400 W
PTE	94.6%	--	94.3%	80%	87%	90.8%
Modulation	MSK	ASK	ASK	OFDM	OFDM	MSK+AM
Data Rate	1 Mbps/ 1 Mbps	20 kbps/ 300 kbps	1 Mbps	4 × 85 kbps/ 4 × 85 kbps	170 kbps/ 170 kbps	1 Mbps/1 Mbps 20 kHz
Number of Data Channel	2	2	1	4	2	3
Complexity	Medium	Low	Medium	High	High	Medium
Hardware cost	Medium	Low	Medium	Medium	High	Medium
Scalability	Medium	Low	Low	High	High	Medium
Analog and Digital Transmission	NO	NO	NO	NO	NO	Yes

PTE：Power Transfer Efficiency； OFDM：Orthogonal Frequency-Division Multiplexing； ASK：Amplitude Shift Keying.

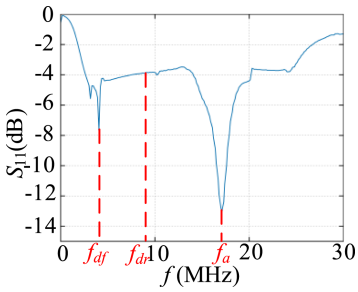

Fig. 9. Trend of impedance Z variation with frequency f.

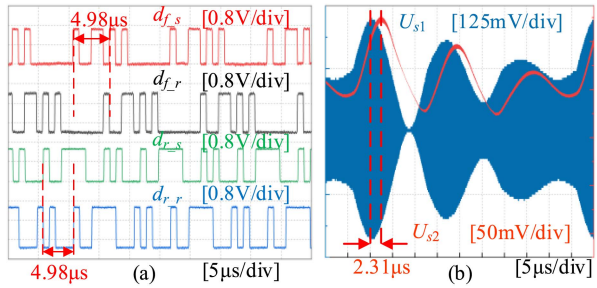

Fig. 11. Signal waveforms. (a) Bidirectional digital signal transmission waveforms. (b) Analog signal transmission waveforms.

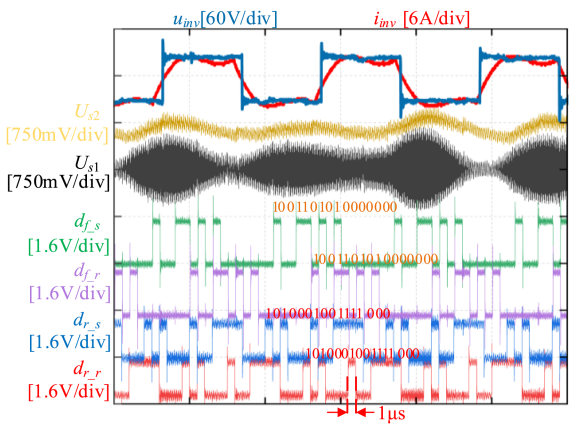

Fig. 10. Waveforms of power transmission and simultaneous analog–digital hybrid signal transmission.

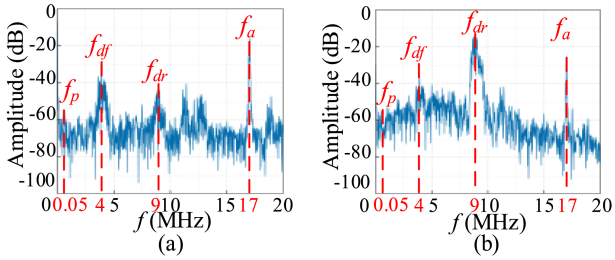

Fig. 12. Spectrum. (a) Spectrum of U_{RXs}. (b) Spectrum of U_{RXp}.

analog and digital signals, the frequency bands are reasonably allocated. As shown in Fig. 9 , the carrier frequencies for digital signal transmission, f_{df} and f_{dr}, are set to 4 and 9 MHz. The actual circuit input return loss impedance S_{11} as a function of frequency f, measured by a network analyzer, is shown in Fig. 9. From Fig. 9, S_{11} reaches its minimum values at 4 and 17 MHz, indicating that the system achieves impedance matching at these frequencies. Therefore, the carrier frequency f_{a} for the analog signal is set to 17 MHz.

B. Experimental Results

The waveforms for power transmission and simultaneous transmission of analog–digital hybrid signals in the SWPDT system are shown in Fig. 11. The input power of the system is 420.0 W, the output power at the load ends is 381.6 W, and the system efficiency is 90.8%

The oscilloscope displays the forward and reverse transmission of digital signals, as shown in Fig. 11(a). The transmission rate of the digital signals is 1 Mbps, with a transmission delay of 4.98 μs. The waveforms of AM modulation and demodulation are shown in Fig. 11(b), where U_{s1} is the output waveform after AM modulation, directly generated by the signal generator. U_{s2} is the analog signal output after envelope detection demodulation. The delay for AM modulation and demodulation is 2.31 μs. The spectrum of the received signal in the SWPDT system is shown in Fig. 12. The gain of the power transmission channel is below -40 dB.

The experimental results indicate that power transmission does not interfere with communication transmission, and the system can achieve distortion-free transmission of both analog and digital signals while power is being transmitted.

C. Comparison With Other Methods

The comparison between the proposed system and previous studies is shown in Table II. Compared with other studies, the proposed system achieves the transmission of two digital signals and one analog signal while transferring power.

IV. Conclusion

This letter proposes an underwater simultaneous wireless power and analog–digital hybrid signal transmission system based on coaxial coils. Compared with conventional systems, it achieves simultaneous transmission of both analog and digital signals while maintaining the high accuracy of digital signals and the continuity of analog signals. The use of analog modulation and envelope detection for analog signal modulation and demodulation reduces the need for additional ADCs, significantly decreases the occupied bandwidth, and improves bandwidth utilization efficiency. The system is structurally simple and has certain feasibility and cost-effectiveness in practical applications. The adopted coaxial coil structure offers advantages of simple fabrication and easy assembly. Experimental results demonstrate successful implementation with 400 W power transmission, 1 Mbps bidirectional digital communication, and 20 kHz unidirectional analog signal transmission. The system effectively eliminates interference between power transmission and signal communication channels.

References

[1] Y. Feng, Y. Sun, T. Lin, H. Hu, and F. Chen, "Mutual inductance surrogate model of the UWPT system and its constant power optimization at misaligned positions," *Wirel. Power Transfer*, vol. 11, no. 1, 2024, Art. no. e001.

[2] B. Luo et al., "Front-end parameter identification method based on Adam-W optimization algorithm for underwater wireless power transfer system," *IEEE Trans. Power Electron.*, vol. 40, no. 4, pp. 6307–6318, Apr. 2025.

[3] Z. Wu, L. Tan, X. Hu, Z. Yuan, and X. Huang, "A three-channel M-ary simultaneous wireless power and data transfer system," *IEEE Trans. Ind. Electron.*, vol. 72, no. 5, pp. 5440–5451, May 2025.

[4] T. Li, Z. Sun, Y. Wang, J. Mai, and D. Xu, "An underwater simultaneous wireless power and data transfer system with 1-Mbps full-duplex communication link," *IEEE Trans. Ind. Informat.*, vol. 20, no. 2, pp. 2620–2631, Feb. 2024.

[5] C. Da, L. Wang, F. Li, C. Tao, and Y. Zhang, "Analysis of undersea simultaneous wireless power and 1 Mb/s data rate transfer system based on DDQ coil," *IEEE Trans. Power Electron.*, vol. 38, no. 10, pp. 11814–11825, Oct. 2023.

[6] P. Gjanci, C. Petrioli, S. Basagni, C. A. Phillips, L. Bölöni, and D. Turgut, "Path finding for maximum value of information in multi-modal underwater wireless sensor networks," *IEEE Trans. Mob. Comput.*, vol. 17, no. 2, pp. 404–418, Feb. 2018.

[7] J. Li, X. Zhang, and X. Tong, "Research and design of misalignment-tolerant LCC–LCC compensated IPT system with constant-current and constant-voltage output," *IEEE Trans. Power Electron.*, vol. 38, no. 1, pp. 1301–1313, Jan. 2023.

[8] Y. Luo, Y. Yang, H. Hong, and Z. Dai, "A simultaneous wireless power and data transfer system with full-duplex mode for underwater wireless sensor networks," *IEEE Sens. J.*, vol. 24, no. 8, pp. 12570–12583, Apr. 2024.

[9] C. Da, F. Li, L. Wang, C. Tao, S. Li, and M. Nie, "Pulse synchronization scheme for undersea BWPT system based on simultaneous wireless power and data transfer technology," *IEEE Trans. Circuits Syst. II Exp. Briefs*, vol. 72, no. 1, pp. 333–337, Jan. 2025.

[10] Y. Jing, X. Dan, J. Yu, K. Fu, and S. M. Sharkh, "Simultaneous wireless power and multi-channel data transmission based on OFDM," *IEEE Trans. Power Electron.*, vol. 39, no. 7, pp. 8894–8903, Jul. 2024.

[11] Y. Jing, K. Fu, J. Yu, X. Dan, S. Ni, and S. M. Sharkh, "Simultaneous wireless power and data transfer system with full-duplex mode based on half-cycle OFDM," *IEEE Trans. Ind. Electron.*, vol. 72, no. 2, pp. 1412–1421, Feb. 2025.